Scientific Research Publishing

Materials Sciences and Applications, 2024, 15, 253-269
https://www.scirp.org/journal/msa
ISSN Online: 2153-1188
ISSN Print: 2153-117X

Antimicrobial Activity, Structural, Crystallographic and Thermal Characteristics of Alpha-Titanium Phosphate Promoted by Silver Ions

Enzo Erbisti Garcia[1*], Agnes Maria Cupertino Fernandes Araujo[2], Gerson Alberto Valencia Albitres[1], Daniela de França da Silva Freitas[1], Danielle Mattos Mariano[1], Carlos Magno Fialho Soares[1], Sibele Piedade Cestari[3], Marco Antônio Lemos Miguel[2], Luis Claudio Mendes[1]

[1]Institute of Macromolecules Professora Eloisa Mano, Federal University of Rio de Janeiro, Avenida Horacio Macedo, 2030, Centro de Tecnologia, Bloco J, Ilha do Fundão, Rio de Janeiro, Brazil
[2]Institute of Microbiology Paulo de Góes, Federal University of Rio de Janeiro, Centro de Ciencias da Saude, Bloco I, Ilha do Fundão, Rio de Janeiro, Brazil
[3]Innovation in Polymer Engineering (PIEP), University of Minho, Guimarães, Portugal
Email: *enzoerbisti@ima.ufrj.br

How to cite this paper: Garcia, E.E., Araujo, A.M.C.F., Albitres, G.A.V., de Freitas, D.F.S., Mariano, D.M., Soares, C.M.F., Cestari, S.P., Miguel, M.A.L. and Mendes, L.C. (2024) Antimicrobial Activity, Structural, Crystallographic and Thermal Characteristics of Alpha-Titanium Phosphate Promoted by Silver Ions. *Materials Sciences and Applications*, **15**, 253-269.
https://doi.org/10.4236/msa.2024.158018

Received: July 16, 2024
Accepted: August 18, 2024
Published: August 21, 2024

Copyright © 2024 by author(s) and Scientific Research Publishing Inc.
This work is licensed under the Creative Commons Attribution International License (CC BY 4.0).
http://creativecommons.org/licenses/by/4.0/

Open Access

Abstract

The recent global spread of the pandemic underscores the necessity of seeking new materials effective against microorganisms. Nanotechnology offers avenues for developing multifunctional materials. In this study, alpha-titanium phosphate (α-TiP) nanoparticles were synthesized and treated with silver salt to enhance their antimicrobial properties. The physicochemical characteristics and antimicrobial activity were evaluated. It was revealed by X-ray diffraction analysis that the structural integrity of α-TiP was influenced by ethylenediamine and silver ions. Distinct degradation profiles for each chemical modification were shown by thermogravimetric analysis. Infrared spectroscopy detected shifts and new absorption peaks in the spectra depending on the type of modification. Energy dispersive spectroscopy confirmed the disaggregation of α-TiP galleries following the addition of silver salt, which increased their effectiveness against microorganisms. Notably, only the sample treated with silver ions exhibited antimicrobial action. Antimicrobial activity was tested against the bacteria of medical importance *Escherichia coli*, *Salmonella* Enteritidis, *Pseudomonas aeruginosa*, *Staphylococcus aureus*, *Bacillus cereus*, *Listeria momocytogenes* and the yeast *Candida albicans*. All microorganisms were inhibited by sample containing silver. Minor inhibition was observed against the Gram-positive bacteria *L. monocytogenes* and *Bacillus cereus*, while the

greatest inhibition occurred against the fungus (yeast) *C. albicans*. The results revealed a potential application of the nanoparticles for control of microorganisms in public health.

Keywords

Titanium Phosphate, Silver Nitrate, Antimicrobial Action

1. Introduction

The emergence of nanotechnology has broken new ground in various techno-scientific fields. The use of natural or synthetic nanometric compounds has facilitated greater multidisciplinarity and integration over different sectors, including biology, physics, chemistry, mechanics, and materials science. Over the past decade, transition metal phosphate materials have emerged as key components in various functional devices. Renowned for their affordability, abundance, and eco-friendliness, transition metal phosphates offer numerous advantages. Their inherent stability, along with unique chemical and physical properties, makes them highly desirable for a wide range of applications.

Furthermore, their multifunctionality can be finely adjusted to meet specific requirements. The structural diversity of transition metal phosphates significantly impacts their properties. Ranging from 1D nanowires to 3D nanostructures, each configuration displays distinct characteristics. Titanium and zirconium are commonly found in compounds used to synthesize lamellar phosphates. These phosphates demonstrate immense potential across various fields. From catalysis to ion exchange, and even as fillers in polymer composites, their versatility is boundless. Chemically modifying their interlayer spacing further expands their utility, enabling the creation of devices for proton conduction, drug delivery, energy storage, sensors, biosensors, flame retardants, and beyond [1] [2]. Despite zirconium phosphates historically dominating the field of lamellar solids among tetravalent metal phosphates since the 1950s, titanium laminar phosphates emerged as significant contenders approximately a decade later, attracting notable attention. In the literature, three nanolayered titanium phosphates have been documented thus far. The crystalline α-$Ti(HPO_4)_2{\cdot}H_2O$ (α-TiP) mirrors the structure of its zirconium counterpart (α-ZrP), signifying its equivalence. Another intriguing dihydrate layered material is γ-titanium phosphate (γ-TiP), formulated as γ-Ti $(HPO_4)_2{\cdot}2H_2O$ or later as γ-$Ti(PO_4)(H_2PO_4){\cdot}2H_2O$. γ-TiP display a larger interlayer spacing than α-TiP due to the presence of two interlayer water molecules. It shares an iso-structure with γ zirconium phosphate, as do its dehydrated forms known as β-TiP [β-$Ti(PO_4)(H_2PO4)$] and β-ZrP [β-$Zr(PO_4)(H_2PO_4)$]. The applications of α-TiP and γ-TiP are diverse, including ion exchange, catalysis, ionic conductivity, and serving as electrodes for Li- and Na-ion storage. Furthermore, they can be functionalized with organic species and exfoliated. However, their utilization in biologically relevant applications remains largely unexplored [3]. These layered tetra-

valent metal phosphates, characterized by strong bonds in two dimensions and weaker bonds in the third, undergo two primary chemical reactions. Firstly, intercalation reactions maintain the two-dimensional bonding while expanding the interlayer spacing sufficiently to absorb guest molecules. This preserves crystallinity or semi-crystallinity due to absorptive interactions between the guest and host sheets. Secondly, exfoliation represents an extreme form of intercalation, where weakly attractive or even repulsive forces between sheets result in easily separable (nano) sheets, facilitated by solvent molecules. These distinctive properties and reactions underscore the diverse potential applications of titanium and zirconium phosphates, spanning from catalysis, drug delivery, and proton conductivity to photochemistry, and polymer nanocomposites. Understanding their structural nuances opens avenues for innovative advancements across multiple fields [4]-[7]. Due to the increase of microorganisms' resistance to substances used for combating clinical infections or environmental decontamination more and more researchers have increased interest in finding new and promising materials with antimicrobial action [8]-[10]. An increasing number of researchers are showing interest in discovering promising materials with antiseptic and/or sanitizing properties. Silver particles and ions, due to their size and mobility, are utilized in medicinal and pharmaceutical applications, including cosmetic and personal hygiene products [11]. Nekooei-Fard *et al*. prepared films (0.1 mm) of ethylene-vinyl acetate copolymer (EVA) embedded with zeolite modified with silver, zinc and copper ions. The sample containing silver-zeolite showed the greatest antimicrobial activity against *Escherichia coli*, *Staphylococcus aureus*, and *Candida albicans*. [12]. Nasiri *et al*. synthesized a kind of new antibiotic by encapsulating silver nanoparticles with Arabic gum, under microwave heating. Antibacterial and antifungal evaluations revealed action against *Escherichia coli*, *Staphilococcus aureus* and *Aspergillus flavus* mycelia [13]. Karci *et al*. synthesized a silver complex through the reaction of silver oxide with benzimidazolium salts and assessed its performance as an antimicrobial agent. Effective action was revealed for *Escherichia coli*, *Staphilococcus aureus* and *Pseudomonas aeruginosa* [14]. The health security of the population drives the growing demand for materials with antiseptic and/or sanitizing properties. In this study, α-TiP nanoparticles were synthesized and modified with silver salt. The physicochemical characteristics and antimicrobial activity were evaluated.

2. Materials and Methods

2.1. Materials

The materials utilized in this study included phosphoric acid (85%), titanium isopropoxide (97%), absolute ethanol, ethylenediamine (EDA, 99%), ethylenediaminetetraacetic acid (EDTA, 99%) and silver nitrate, obtained from Sigma-Aldrich.

2.2. Alpha-Titanium Phosphate (α-TiP) Synthesis, Pre-Expansion and Silver Modification

The synthesis of α-TiP was based on the mixing of titanium isopropoxide and

phosphoric acid in a 1:8 molar ratio, along with deionized water, at 120˚C, with vigorous stirring for 24 hours. After that, the product was washed until reaching q pH of 6 [15]. The pre-expansion of α-TiP galleries was carried out using ethylenediamine (EDA) at an amine:phosphate ratio of 2:1. The EDA solution was added to the aqueous dispersion of TiP, under magnetic stirring and left for 24 hours. Subsequently, the liquid medium was evaporated and the remaining solid was named TiPEDA [15]. To functionalize TiPEDA, EDTA (1.23 g) was dissolved in a slightly alkaline aqueous solution of sodium carbonate (0.63 g/80 ml) and it was added to the aqueous dispersion of TiPEDA (1 g), at 25˚C, under magnetic stirring for 24 hours. Thereafter, the aqueous medium was filtered and the solid was dried in an oven at 70˚C. The sample was designated as TiPEDAEDTA. Finally, the last one was modified with silver nitrate. An aqueous solution of silver salt (0.7 g $AgNO_3$/100 mL) was prepared and added dropwise to an aqueous dispersion of TiPEDAEDTA under stirring for 24 hours. The solution was then filtered, and the solid was dried. The resulting sample was named TiPEDAEDTAAg.

2.3. Wide Angle X-Ray Diffractometry (WAXD)

Diffraction analysis was carried out in a Rigaku Ultima IV diffractometer using 40 kV, 20 mA, step of 0.05, 2θ angle ranging from 2˚ to 40˚.

2.4. Thermogravimetric Analysis (TGA)

TGA data was acquired throughout TA analyzer model Q500, between 30˚C - 700˚C, at 10˚C·min^{-1}, under a nitrogen atmosphere. The final degradation temperature - T_{final} -, the temperatures where the degradation speed was maximum - T_{max}—and where the mass loss was 5, 10, 25 and 50 wt.% - T_5, T_{10}, T_{25}, T_{50}, - were registered.

2.5. Fourier Transform Infrared Spectroscopy (FTIR)

The infrared evaluation was performed in Perkin-Elmer equipment, model Frontier MIR/FIR, within the range of 4000 - 400 cm^{-1}. The spectra were obtained by attenuated total reflectance (ATR), using 60 scans and a resolution of 4 cm^{-1}.

2.6. Field Emission Scanning Electron Microscopy and Energy Dispersive Spectroscopy (FESEM/EDS)

The transverse section SEM images were captured using a Tescan field emission microscope, model MIRA 4 LMU (LowVac Mode UniVac™) equipment, voltage of 10 kV). Elemental analysis was performed with an EDS detector equipped with a 30 mm^2 Si_3N_4 window, with a resolution lower than 129 eV for the MnKα emission line.

2.7. Microbiological Evaluation

Origin and preparation of microorganisms: Gram-positive and Gram-negative

bacteria were used which differ due to the chemical composition of the cell wall. As Gram-negative bacteria were tested, *Escherichia coli* from American Type Culture Collection (ATCC) 11229, *Salmonella* Enteritidis 13076 and *Pseudomonas aeruginosa* ATCC 15442. Gram-positive bacteria tested were *Staphylococccus aureus* ATCC 29213, *Listeria monocytogenes* ATCC 19117 and *Bacillus cereus* ATCC 14579. The Yeast (fungus) *Candida albicans* ATCC 10231 was also included. All microorganisms belonging to the culture collection of the Institute of Microbiology Paulo de Góes at UFRJ. These microorganisms were selected due to their frequent involvement in clinical infections or foodborne diseases in humans. The microorganisms were stored under refrigeration and were activated for the experiments. The bacteria were activated by cultivation in 5 ml of liquid culture medium - Brain Heart Infusion (BHI -Merck) for 24 h. *Candida albicans* was propagated in Saboraud Broth (Merck) for 48 h. Both bacteria and yeast were incubated at 37˚C.

Test of antimicrobial activity: after activation, the strains were streaked across the surface on BHI agar (Merck) and Saboraud agar (Merck) plates and incubated at 37˚C to obtain isolated colonies. From each microorganism, approximately 5 colonies were used to prepare a suspension in sodium chloride solution 0.85% (w/v) to reach a cell concentration of approximately 10^8 colony-forming units per milliliter (CFU/ml). From the suspensions, microorganisms were inoculated directly onto the surface of BHI agar or Saboraud agar plates, for bacteria and yeast, respectively. The inoculum was made with a sterile swab (wooden rod with cotton tip) in 3 different directions, to achieve confluent microbial growth. Immediately after the inoculum, ten microliters of a colloidal water solution of different samples: TiP, TiPEDAEDTA and TiPEDAEDTAAg (1:1 w/v) in sterile distilled water were deposited above the microorganisms. Plates were incubated at 37˚C for 24/48 hours. Tests considered as positive presented a zone of inhibition of microbial growth around the deposited samples. Zones of inhibition were measured in millimeters. All tests were performed in triplicate.

3. Results and Discussion

3.1. Wide Angle X-Rays Diffractometry (WAXD)

Diffractograms of the precursors ($AgNO_3$ and α-TiP) (**Figure 1**) and modified phosphates (TiPEDA, TiPEDAEDTA, TiPEDAEDTAAg) (**Figure 2**) are presented. The $AgNO_3$ diffraction pattern showed a low-intensity diffraction angle at 21.9˚ and a high-intensity peak near 36˚, consistent with findings reported by Hou *et al*. and Aziz *et al*. [16] [17]. The diffraction angle at $2\theta = 12.05^\circ$ corresponded to alpha-titanium phosphate (α-TiP, d002 ≈ $d_{spacing}$ = 0.75 nm), as reported Amghouz *et al*., Wang *et al*. and Ortiz-Oliveros *et al*. [18]-[20]. After modification with EDA, the basal peak of α-TiP disappeared, but a new plane at $2\theta = 8.4^\circ$ with a $d_{spacing}$ of 1.05 nm was observed. This indicates the successful expansion of α-TiP galleries. Peng *et al*. also modified α-TIP with different diamines. and observed a peak at 9.84 Å for EDA. Additionally, the authors noted that the expansion of α-TiP galleries depended on the length of the diamine chain [21]. Although similar, the diffractograms of TiPEDA and TiPEDAEDTA

displayed diffraction angles with lower intensity. TiPEDAEDTAAg exhibited a total absence of diffraction angles, indicating that the silver salt promoted the disruption of the phosphate arrangement. It can be inferred that the presence of EDTA fostered a stronger interaction between the modified phosphate and the silver salt, resulting in structural disaggregation.

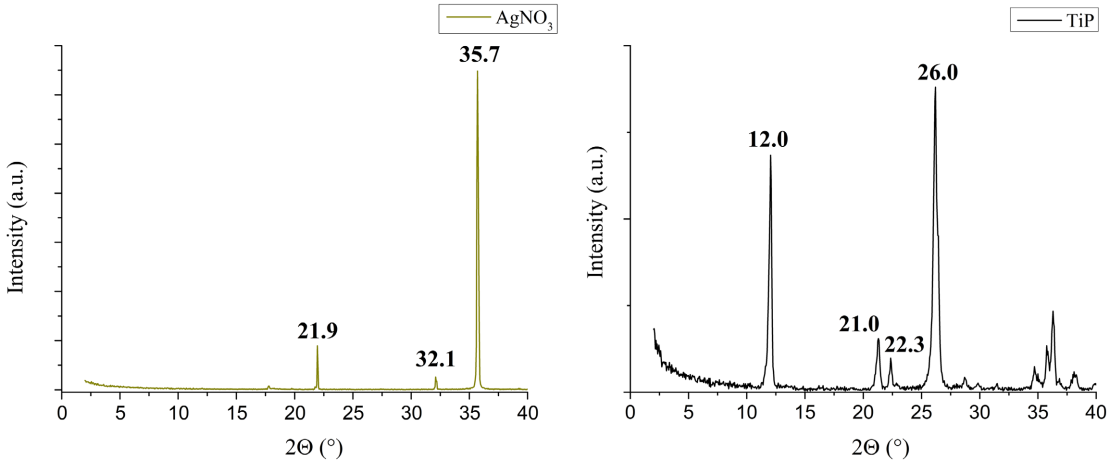

Figure 1. WAXD curves of $AgNO_3$ and α-TiP.

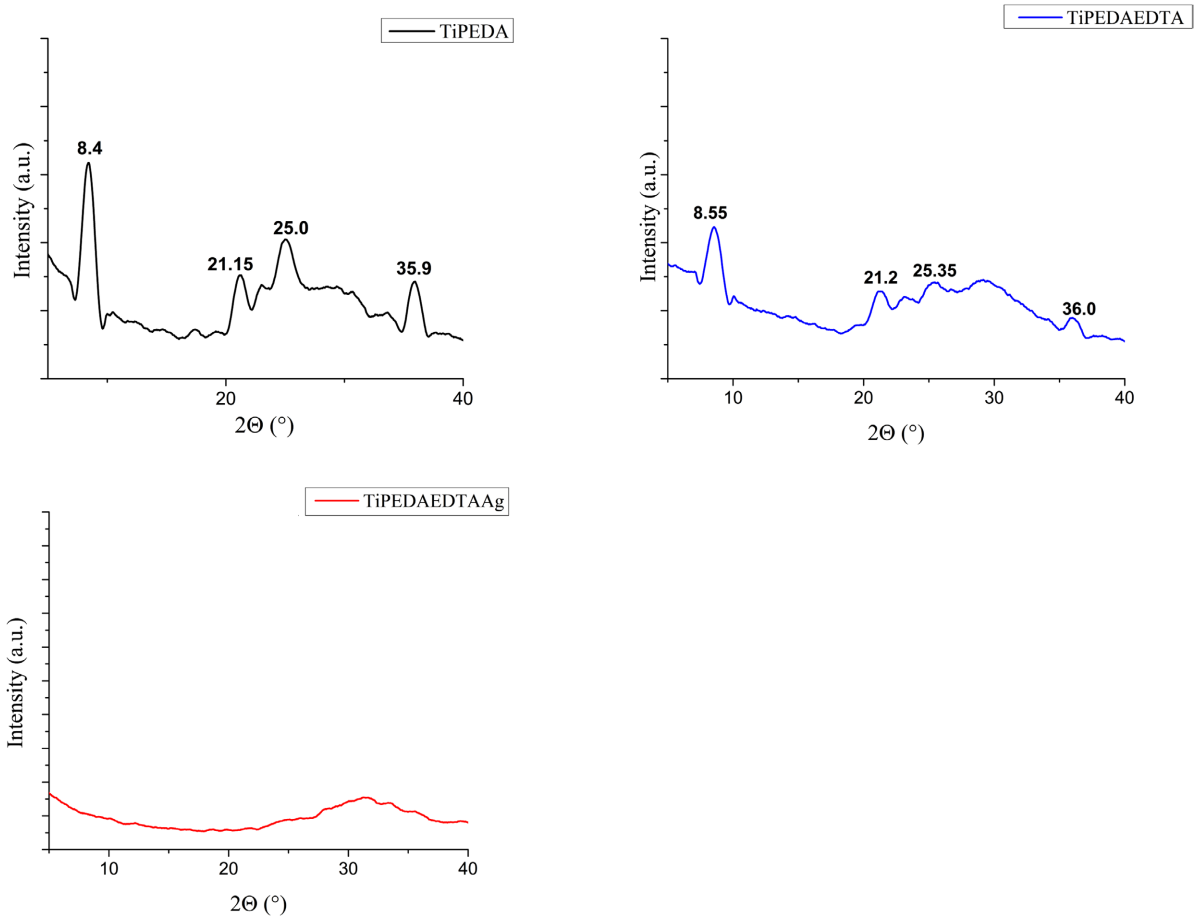

Figure 2. WAXD curves of TiPEDA, TiPEDAEDTA and TiPEDAEDTAAg.

3.2. Thermogravimetric Analysis (TGA)

Figures 3(a)-(c) illustrate the TG/DTG curves of the precursors as well as the pristine and modified phosphate. The *α*-TiP mass loss curve displayed one decay between 200˚C - 300˚C and a second one around 400˚C - 500˚C. Similarly, two decays were observed for TiPEDA: one below 100˚C and another between 300˚C - 400˚C. TiPEDAEDTA exhibited a similar behavior. At least two degradation decays were noticeable in the mass loss curve of TiPEDAEDTAAg. The derivative curve of EDTA revealed two stages of degradation, with an intense peak at 259˚C and another at 375˚C with very low intensity. Narayanan *et al*. synthesized a new water-absorbing material based on an adduct of EDTA-Urea cross-linking with chitosan. EDTA's thermogravimetric data indicated stability up to 200˚C, but between 230˚C - 320˚C, approximately 70% of the mass was released [22]. Basically, $AgNO_3$ displayed a prominent degradation stage with a maximum at 489˚C, accompanied by a small shoulder around 530˚C. In their work on non-isothermal decomposition of $AgNO_3$ Jankovic *et al.* identified two degradation stages at 468˚C and 508˚C. The first stage was attributed to its boiling point followed by decomposition, while the second one was linked to the degradation endpoint [23]. *α*-TiP exhibited two degradation stages. The first, with a maximum around 200˚C, was associated with water within the crystalline lattice, while the final one, with a maximum at 492˚C, was related to the transformation of phosphate into pyrophosphate. Two degradation stages were detected for TiPEDA. The release below 100˚C was attributed to residual amine and/or solvent, while the one at 358˚C was ascribed to the release of bonded amine. In the case of TiPEDAEDTA, an initial degradation stage at 54˚C was assigned to the release of residual solvent. The latter stage consisted of a shoulder at 258˚C, related to EDTA degradation, and a peak at 369˚C, representing the release of bonded amine. The derivative curve of TiPEDAEDTAAg resembled that of TiPEDAEDTA but an additional degradation stage was revealed around 550˚C, ascribed to the coordination of EDTA and silver ions. Table 1 displays the temperature evolution correspondingto 5, 10, 25 and 50% of mass loss. EDTA released 50% of its mass until 266˚C, with an additional 42% lost in a second degradation stage. For $AgNO_3$, 25% of mass loss was occurred at 483˚C, followed by an additional 16% lost until reaching the endpoint temperature of 552˚C. *α*-TiP exhibited 10% mass loss up to 448˚C, with an additional 6% released until reaching the endpoint temperature. For TiPEDA, 10% mass loss occurred at 69˚C, with an additional 20% lost thereafter, representing the content of anchored EDA. TiPEDAEDTA presented 10% mass loss at 170˚C. The progress of the run indicated additional mass loss of 18%, attributed to the release of degradation products from EDA and EDTA. The TiPEDAEDTAAg sample experienced 5% mass loss at 135˚C. By the end of the run, an additional 10% mass loss was detected, associated with degradation matter of EDA, EDTA, and their coordination with silver ions. The results corroborated with those obtained from WADX.

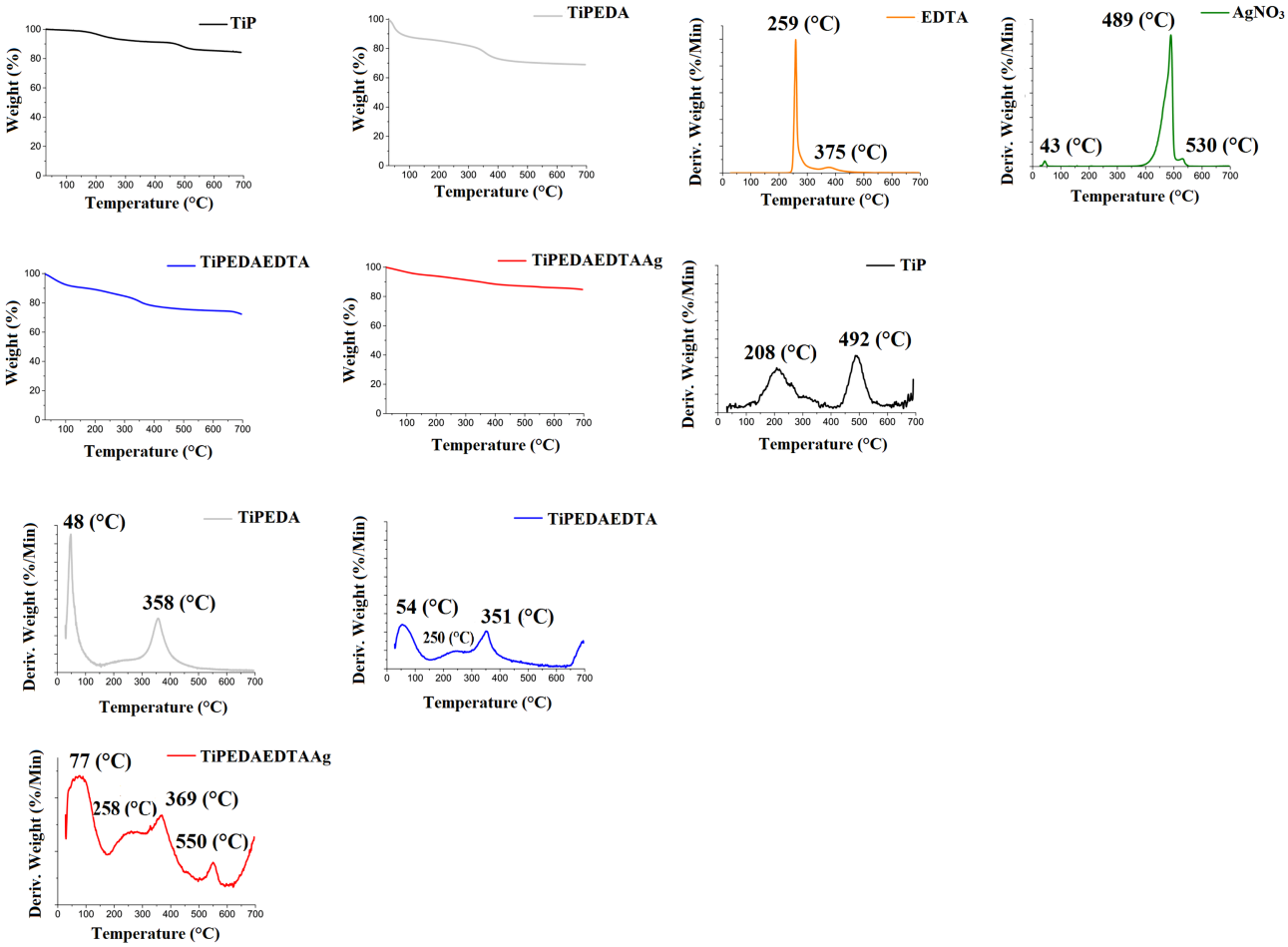

Figure 3. Mass loss curves of TiP, TiPEDA, TiPEDAEDTA and TiPEDAEDTAAg (a). Derivatives curves of EDTA, $AgNO_3$ and *α*-TiP (b). Derivative curves of TiPEDA, TiPEDAEDTA and TiPEDAEDTAAg (c).

Table 1. TGA data of the precursors, pristine and modified *α*-TiP.

Sample	T_5 (˚C)	T_{10} (˚C)	T_{25} (˚C)	T_{50} (˚C)	T_{max} (˚C)	T_{final} (˚C)	Residue (%)
EDTA	251	254	258	266	259/375*	432	8
$AgNO_3$	440	459	483	-	489/530*	552	59
TiP	226	448	-	-	208/492	551	84
TiPEDA	47	69	370	-	48/358	553	70
TiPEDAEDTA	67	170	469	-	54/250*/351	552	72
TiPEDAEDTAAg	135	344	-	-	77/258-369*/550	583	85

*Shoulder.

3.3. Infrared Spectroscopy (FTIR)

Figure 4(a) identifies the main absorptions of the precursors and modified *α*-TiP across the entire range of FTIR spectra. EDTA presents absorptions at

3017 - 2865 cm^{-1} (C-H and OH); 1695 cm^{-1} (C=O); 1441 cm^{-1} (O=C-OH); 1391 cm^{-1} (C-OH); 1007 cm^{-1} (N-C) and 965 cm^{-1} (C–C). These assignments are in agreement with those reported by Magdalena *et al.* in their study on functionalization of EDTA with magnetite [24]. Absorptions at 3455; 2428; 1763; 1385 and 824 cm^{-1} were recorded for $AgNO_3$. Augustine *et al.* attributed the band at 1385 cm^{-1} to the symmetric vibration of the nitro compound in the work on green synthesis of silver nanoparticles [25]. *α*-TiP showed absorptions around 3554 and 3476 cm^{-1}, which are related to the symmetric and asymmetric stretching of the hydrogen bond between the P-O-H groups and adsorbed water. A peak was observed at 1617 cm^{-1}, corresponding to the H-O-H vibration of water confined within the crystal lattice. Additionally, absorptions at 1255, 1115, 1033, 1013, 970 cm^{-1} were attributed to the stretching of P-O_4^-, P-O and P-O-H groups. Absorptions at 615, 542, and 423 cm^{-1} were ascribed to P-O-H and Ti-O linkages, as reported by Garcia *et al.* [26]. Following pre-expansion with ethylenediamine, *α*-TiP exhibited shifted and newly appeared absorptions. The absorptions around 3554 and 3476 cm^{-1} were displaced to 3430 and 3037 cm^{-1} due to the reaction between P-O-H groups in the titanium phosphate and amine groups in the $_2HN$-CH_2-CH_2-NH_2 resulting in the formation of the -PO^- $^+{}_3HN$- amine salt. New absorptions emerged at 2927 cm^{-1} (CH and NH stretching), 1464 cm^{-1} (CH and NH stretching), 1540 and 1512 cm^{-1} ($^+$N-H deformation) as a result of the insertion of EDA [27]. In the range of 1200 - 500 cm^{-1}, absorptions related to phosphate groups and Ti-O vibration modes were displaced to 982, 789, 630, 546 cm^{-1} [21]. Upon the subsequent insertion of EDTA, the absorptions at 3430 and 3037 cm^{-1} were displaced to 3402 and 3053 cm^{-1} and those ones at 1441 and 1391 cm^{-1} were shifted to 1411 and 1385 cm^{-1}. We believed that these changes could be imputed to a new hydrogen bond between N-H and carbonyl groups in the PO^- $^+$3HN- amine salt and EDTA, respectively. When silver salt was added, the absorptions in the range of 4000 - 3000 cm^{-1} were shifted to 3436 and 3197 cm^{-1} and the appearance of new absorption at 1527 cm^{-1} (C=O-O^- asymmetric stretching) were ascribed to the formation of silver carboxylate salt. In **Figure 4(b)**, the FTIR spectra highlight the spectral regions where their shapes were significantly modified due to each *α*-TiP chemical modification. Between 4000 - 2600 cm^{-1}, the hydrogen bond between P-O-H groups and H-O-H were affected by the progressive insertion of EDA, EDTA and $AgNO_3$. Absorptions related to C-H vibrations mode in the range of 3000 - 2800 cm^{-1} confirmed the anchoring of those precursors. Similarly, in the region of 1600 - 900 cm^{-1}, the spectra of the modified samples differed notably from that of pristine *α*-TiP. Besides the new absorption at 1527 cm^{-1} the absorption at 1459 cm^{-1} was associated with the vibration modes of C=O-O^- (symmetric stretching) and 1464 cm^{-1} (CH and NH stretching) endorsed that the modifications were successful [27]. These results are in agreement with those observed in WAXD and TGA analyses.

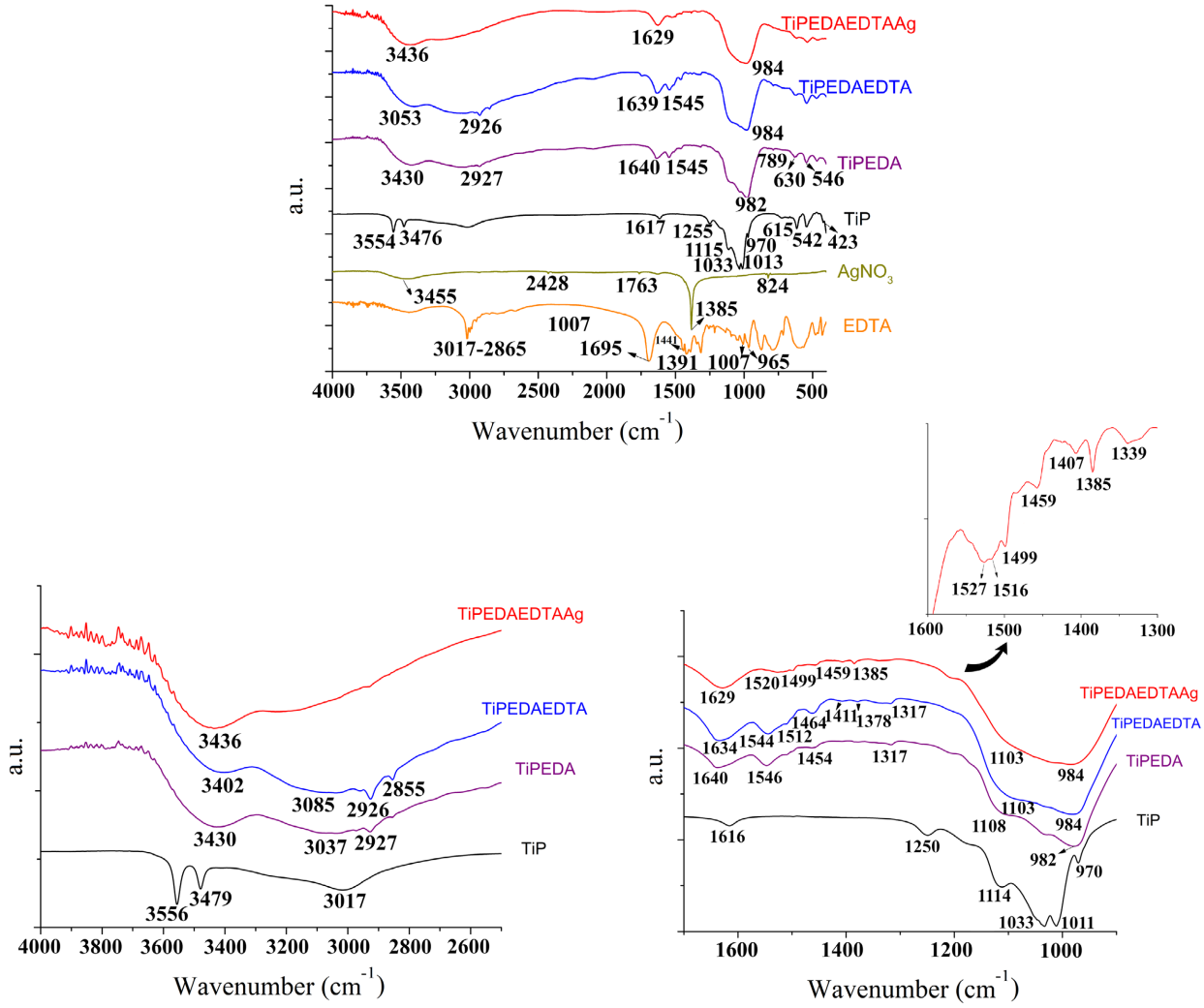

Figure 4. FTIR spectra of the precursors and modified α-TiP: (a) (4000 - 500 cm^{-1}); (b) (4000 - 2600 and 1700 - 1000 cm^{-1}).

3.4. Scanning Electron Microscopy/Energy Dispersive Spectroscopy (SEM/EDS)

Figure 5 shows SEM images of α-TiP and its modifications. α-TiP presents a stacking of defective hexagonal sheets (24.4 nm) with non-homogeneous stack sizes but a smooth surface. The chemically modified samples showed coarse and agglomerated structures compared to α-TiP. **Figure 6** exhibits the evaluation of the elements by energy dispersive X-ray spectroscopy. The quantitative analysis revealed that the incorporation of silver ions was approximately 32%. To understand the dispersion and distribution of α-TiP particles after each modification, approximately 2 grams of sample were burned in an oven at 700˚C for 3 hours. In the EDS analysis depicted in **Figure 7**, the dispersion and distribution of Ti, P, and Ag in each sample are revealed. In the case of α-TiP, Ti and P are homogeneously dispersed and distributed. However, for samples modified with EDA and EDTA, there is little variation in the dispersion and distribution of Ti, while P showed agglomeration, due to the availability of P-O-H group for chemical

modifications. For TiPEDAEDTAAg, the presence of silver ions promoted deagglomeration, showing high dispersion and distribution. These findings corroborate those observed in the WAXD, TGA and FTIR analyses.

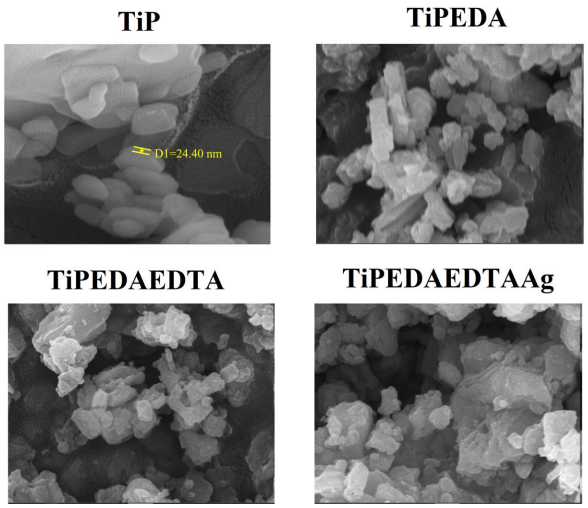

Figure 5. SEM images of *α*-TiP, TiPEDA, TiPEDAEDTA and TiPEDAEDTAAg.

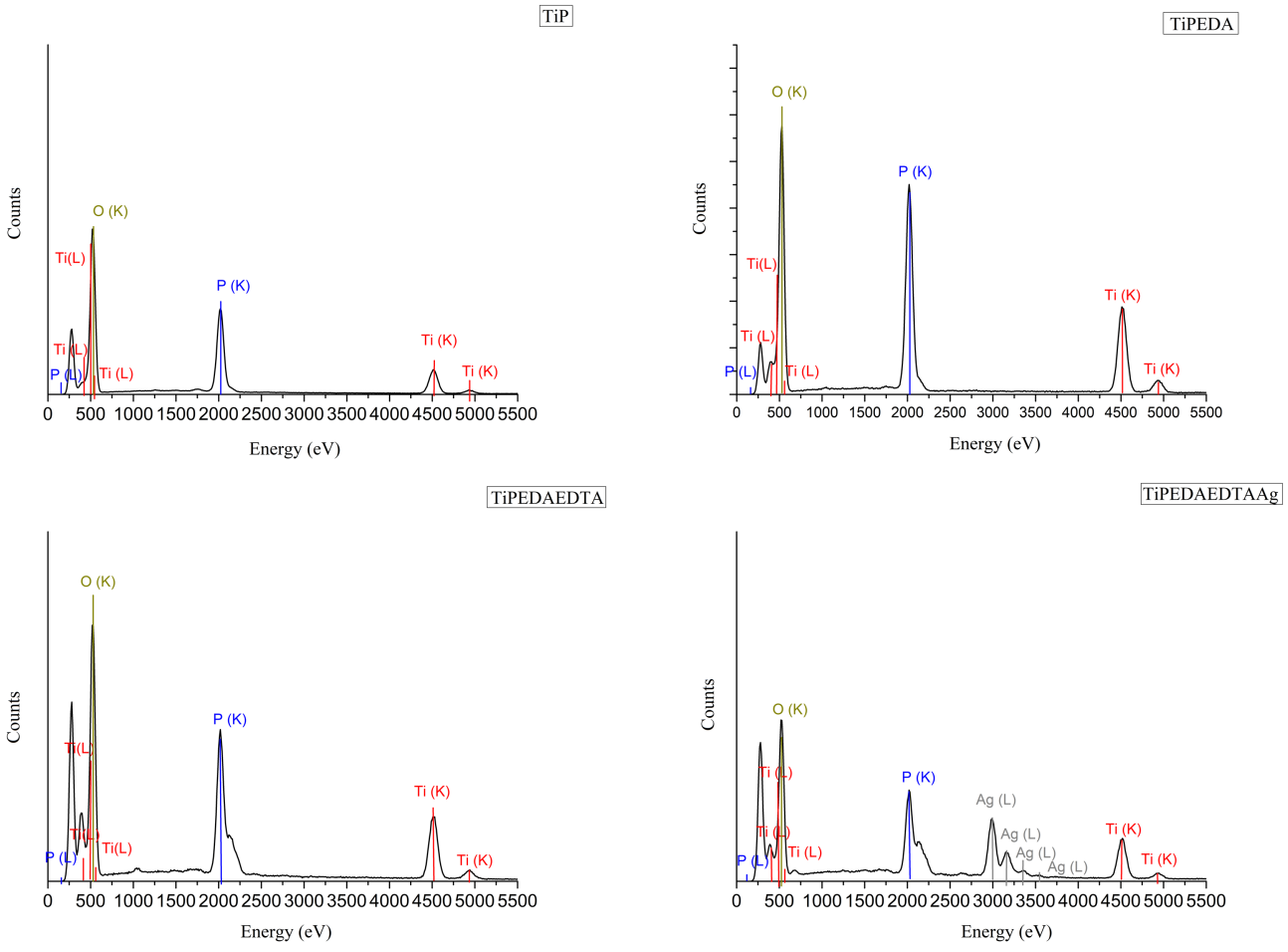

Figure 6. Elemental evaluation by EDS.

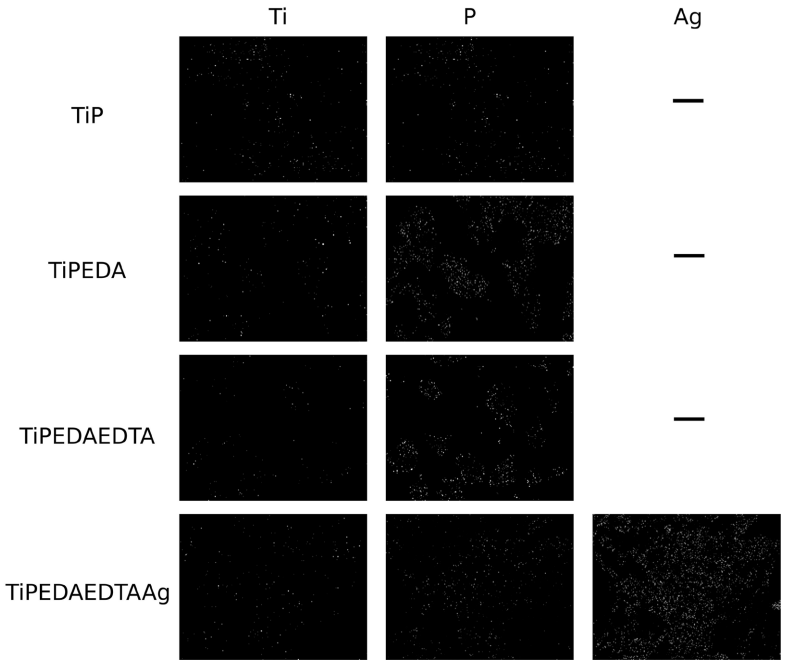

Figure 7. Dispersion and distribution of Ti, P and Ag in each sample.

3.5. Microbiological Evaluation

Over the years, silver has been used as an important alternative to combat microorganisms, which have shown a progressive resistance to antibiotics, antiseptics, and sanitizers applied in therapy or in industrial environments, respectively. The use of silver nanoparticles presents an advantage in more efficient antimicrobial activity in biofilms compared with other methods [28]. Biofilms are microbial communities adsorbed to organic or inorganic matrices, whose structural complexity, in addition to other factors, contributes to increase the difficulty of treatment and eradication on body surfaces or equipment. These evidences motivated the choice of microorganisms to be tested since bacteria such as *Pseudomonas aeruginosa*, *Staphylococcus aureus*, and *Listeria monocytogenes* are recognized for their ability to produce biofilms. In this study, a semi-quantitative screening for antimicrobial activity of silver-containing nanoparticles was carried out. In most tests carried out with silver, a complete zone of microbial inhibition was observed. However, in some cases, outside the inhibition zone, a zone of partial inhibition was also produced. Herein, the inhibition zone was considered only the area of total growth inhibition (**Figure 8**). All microorganisms tested were inhibited only by samples containing TiPEDAEDTAAg (**Table 2**). Exposure to TiP and TiPEDAEDTA did not result in any changes in microbial growth. The smallest zones of inhibition were produced against the Gram-positive bacteria *L. monocytogenes* and *Bacillus cereus*, while the greatest inhibition occurred against the fungus (yeast) *C. albicans*. Similar results were found by Saravam *et al*. when tested the antimicrobial activity of silver nanoparticles against bacteria of medical interest [29]. Herein, the Gram-negatives *Klebsiella pneumoniae* and *Pseudomonas aeruginosa* were more affected than *S. aureus*

and *Staphylococcus epidermidis* (Gram-positive). Kim *et al*. found the Gram-negative *E. coli* and yeast to be more sensitive to silver nanoparticles than *S. aureus* [30]. Although some studies showed greater activity of silver nanoparticles against Gram-negative bacteria when compared to Gram-positive, different results were also found by Rahisuddin *et al*. where the effects on *S. aureus* were more intense than those found against *E. coli*. Also, antifungal activity against the yeasts *Candida albicans*, *C. glabrata*, and *C. tropicalis* was also observed [31]. Manimaram *et al*. in their study found similar susceptibility among Gram-positive and Gram-negative bacteria. No significant differences were found between *K. pneumoniae* and *E. coli* and the Gram-positive *S. aureus* [32]. The variation in the results found in the literature regarding the effects against Gram-negative and Gram-positive bacteria suggests that the antimicrobial activity of silver nanoparticles may depend on different factors, such as the structural characteristics of the preparation of each study, as well as the possibility of being strain-dependent, since different studies used different strains from various origins. In this investigation, although all tested microorganisms were inhibited, *L. monocytogenes* showed the greatest resistance against silver. This result can be justified by its well-studied resistance to unfavorable environmental conditions, including the presence of sanitizers and disinfectants [33]. Belluco *et al*. evaluated the effect of silver on strains of *Listeria monocytogenes* from different origins and found no significant differences among them [34]. Similar results - no resistance to silver-containing nanoparticles in 60 strains of *Listeria monocytogenes* - were achieved by Mohammed & Ziz in an article published on the resistance of Listeria monocytogenes to different antimicrobials [35]. Despite the greater resistance observed for this microorganism, other studies suggested a stability of susceptibility, and consequently, a promising application in the food industry to control this important pathogen.

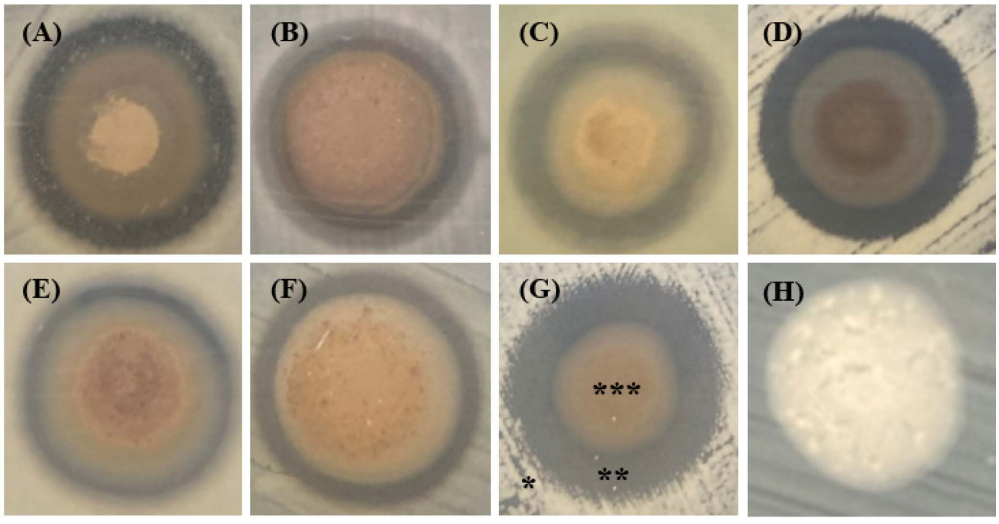

Figure 8. Microrganisms inhibition zone of TiPEDAEDTAAg against bacteria and yeast: (A) *Escherichia coli*, (B) *Salmonella* Enteritidis; (C) *Pseudomonas aeruginosa*, (D) *Staphylococcus aureus*; (E) *Bacillus cereus*; (F) *Listeria monocytogenes*; (G) *Candida albicans*; (H) TiPEDAEDTA; * microbial growth; ** zone of inhibition; *** deposited material.

Table 2. Antimicrobial activity of TiPEDAEDTAAg against bacteria and yeast.

Microorganisms (ATCC[a] number)	Zone of inhibition millimeter[b]
Gram-negative bacteria	
Escherichia coli 11229	11.67 (±0.58)
Salmonella Enteritidis 13076	11.67 (±0.58)
Pseudomonas aeruginosa 15442	11.33 (±0.58)
Gram-positive bacteria	
Staphylococcus aureus 29213	11.00 (±0.58)
Bacillus cereus 14579	10.00 (±0.58)
Listeria monocytogenes 10231	9.33 (±0.00)
Yeast	
Candida albicans 10231	14.00 (±0.00)

[a] American Type Culture Collection; [b] Mean value, n = 3 (the zone of inhibition includes the area in which the suspension has been deposited on the surface of the culture medium (7.71 ± 0.47 millimeter) and the area where microbial growth has been inhibited.

4. Conclusion

Awareness among authorities and international organizations in the health sector has increased, particularly concerning human health in the face of microorganism. The search for materials with aseptic and/or sanitizing properties is in continuous development. In this scenario, α-TiP nanoparticles were synthesized and modified with silver salt. Structure and antimicrobial activity were assessed. The successive chemical modifications induced the increase in the lamellar spacing of α-TiP, allowing for better dispersion and distribution of silver ions on phosphate, and incrementing its antimicrobial action. The findings of antimicrobial activity emerged from the exposure of titanium phosphate modified with silver ions against bacteria and yeast with significant importance in public health, points the need of complementary studies seeking the application of this material in the manufacture of medical or industrially relevant artifacts. In any case, the study showed the potential of silver-modifying titanium phosphate nanoparticles for the control of relevant microorganisms in public health.

Acknowledgements

The authors would like to thank the Conselho Nacional de Desenvolvimento Científico e Tecnológico (CNPq) and FAPERJ - Fundação Carlos Chagas Filho de Amparo à Pesquisa do Estado do Rio de Janeiro - Processo SEI 400724-2023-5 and Universidade Federal do Rio de Janeiro for their support of this research.

Data Availability Statement

All data generated or analysed during this study are included in this published article.

Conflicts of Interest

On behalf of all authors, the corresponding author states that there is no conflict of interest.

References

[1] Zhao, H. and Yuan, Z. (2020) Insights into Transition Metal Phosphate Materials for Efficient Electrocatalysis. *ChemCatChem*, **12**, 3797-3810. https://doi.org/10.1002/cctc.202000360

[2] Tan, S., Yue, J., Tian, Y., Ma, Q., Wan, J., Xiao, Y., *et al*. (2021) In-Situ Encapsulating Flame-Retardant Phosphate into Robust Polymer Matrix for Safe and Stable Quasi-Solid-State Lithium Metal Batteries. *Energy Storage Materials*, **39**, 186-193. https://doi.org/10.1016/j.ensm.2021.04.020

[3] Amghouz, Z., García, J.R. and Adawy, A. (2022) A Review on the Synthesis and Current and Prospective Applications of Zirconium and Titanium Phosphates. *Eng*, **3**, 161-174. https://doi.org/10.3390/eng3010013

[4] Bashir, A., Ahad, S., Malik, L.A., Qureashi, A., Manzoor, T., Dar, G.N., *et al*. (2020) Revisiting the Old and Golden Inorganic Material, Zirconium Phosphate: Synthesis, Intercalation, Surface Functionalization, and Metal Ion Uptake. *Industrial & Engineering Chemistry Research*, **59**, 22353-22397. https://doi.org/10.1021/acs.iecr.0c04957

[5] Wu, L., Wang, H., Kong, X., Wei, H., Chen, S. and Chi, L. (2023) High Strontium Adsorption Performance of Layered Zirconium Phosphate Intercalated with a Crown Ether. *RSC Advances*, **13**, 6346-6355. https://doi.org/10.1039/d2ra07757d

[6] Garcia, E.E., Albitres, G.A.V., Freitas, D.F.S., Mariano, D.M. and Mendes, L.C. (2022) Zinc and Silver Salts-Containing Lamellar Titanium Phosphate: A Multifunctional Filler. *Materials Sciences and Applications*, **13**, 366-388. https://doi.org/10.4236/msa.2022.136021

[7] García-Glez, J., Trobajo, C., Adawy, A. and Amghouz, Z. (2019) Exfoliation and Europium(iii)-Functionalization of A-Titanium Phosphate via Propylamine Intercalation: From Multilayer Assemblies to Single Nanosheets. *Adsorption*, **26**, 241-250. https://doi.org/10.1007/s10450-019-00133-2

[8] Salam, M.A., Al-Amin, M.Y., Salam, M.T., Pawar, J.S., Akhter, N., Rabaan, A.A., *et al*. (2023) Antimicrobial Resistance: A Growing Serious Threat for Global Public Health. *Healthcare*, **11**, Article 1946. https://doi.org/10.3390/healthcare11131946

[9] Maillard, J.-Y. (2007) Bacterial Resistance to Biocides in the Healthcare Environment: Should It Be of Genuine Concern? *Journal of Hospital Infection*, **65**, 60-72. https://doi.org/10.1016/s0195-6701(07)60018-8

[10] Alonso, V.P.P., Furtado, M.M., Iwase, C.H.T., Brondi-Mendes, J.Z. and Nascimento, M.d.S. (2022) Microbial Resistance to Sanitizers in the Food Industry: Review. *Critical Reviews in Food Science and Nutrition*, **64**, 654-669. https://doi.org/10.1080/10408398.2022.2107996

[11] Ahamed, M.S., Ali, M.S., Ahmed, S., Sadia, S.I., Islam, M.R., Rahaman, M.A., *et al*. (2024) Synthesis of Silver Nanomaterials Capping by Fruit-Mediated Extracts and Antimicrobial Activity: A Critical Review. *International Research Journal of Pure and Applied Chemistry*, **25**, 45-60. https://doi.org/10.9734/irjpac/2024/v25i1844

[12] Nekooei-Fard, M., Jahanmardi, R., Fazaeli, R. and Sohrabi-Haghdoost, N. (2023) Effects of Zeolite Loaded with Silver, Copper, or Zinc Ions on Antimicrobial Properties of the Ethylene-Vinyl Acetate Copolymer. *Polymers for Advanced Technolo-*

gies, **35**, e6237. https://doi.org/10.1002/pat.6237

[13] Nasiri, S. and Jafarizadeh-Malmiri, H. (2024) Microwave Irradiation in Green Antimicrobial Silver Nanoparticles Synthesis Using Arabic Gum: Preparation, Optimization and Characterization. *Journal of Chemical and Petroleum Engineering*, **58**, 149-163.

[14] Karci, H., Dündar, M., Nawaz, Z., Özdemir, İ., Gürbüz, N., Koç, A., *et al*. (2024) Sythesis, Characterisation, Anticancer and Antimicrobial Activity of Ag-N-Heterocyclic Carbene Complexes Containing Benzimidazole Derivatives. *Inorganica Chimica Acta*, **565**, Article 121992. https://doi.org/10.1016/j.ica.2024.121992

[15] Albitres, G.A.V., Cestari, S.P., Freitas, D.F.S., Rodrigues, D.C., Mendes, L.C. and Neumann, R. (2019) Intercalation of A-Titanium Phosphate with Long-Chain Amine Aided by Short-Chain Amine. *Applied Nanoscience*, **10**, 907-916. https://doi.org/10.1007/s13204-019-01176-1

[16] Hou, Y., Pan, Y., Dong, C. and Nie, B. (2020) Direct Transformation of Agno3 Complex Encapsulated Fullerene (c60) Microcrystal on Solid Silver Nitrate Crystal without Organic Ligands. *Applied Organometallic Chemistry*, **34**, e5978. https://doi.org/10.1002/aoc.5978

[17] Aziz, S., Abdulwahid, R., Rasheed, M., Abdullah, O. and Ahmed, H. (2017) Polymer Blending as a Novel Approach for Tuning the SPR Peaks of Silver Nanoparticles. *Polymers*, **9**, Article 486. https://doi.org/10.3390/polym9100486

[18] Amghouz, Z., Mendoza-Meroño, R. and Adawy, A. (2023) Nucleation & Growth of A-Ti(HPO4)2·H_2O Single-Crystal and Its Structure Determination from X-Ray Single-Crystal Data. *Journal of Solid State Chemistry*, **327**, Article 124251. https://doi.org/10.1016/j.jssc.2023.124251

[19] Wang, C., Cheng, Q. and Wang, Y. (2018) Anion-Controlled Cation-Exchange Process: Intercalating A-Titanium Phosphate through Direct Ion Exchange with Alkylammonium Salts. *Inorganic Chemistry*, **57**, 3753-3760. https://doi.org/10.1021/acs.inorgchem.7b03030

[20] Ortíz-Oliveros, H.B., Flores-Espinosa, R.M., Ordoñez-Regil, E. and Fernández-Valverde, S.M. (2014) Synthesis of A-Ti(HPO4)2·H_2O and Sorption of Eu (iii). *Chemical Engineering Journal*, **236**, 398-405. https://doi.org/10.1016/j.cej.2013.09.103

[21] Peng, W., Wang, X., Wang, M., Wang, Y. and Cheng, Q. (2020) Embedding Alkyldiamine into Layered A-Titanium Phosphate via Direction Exchange and Its Application in Euiii Removal from Water. *Zeitschrift für anorganische und allgemeine Chemie*, **646**, 399-406. https://doi.org/10.1002/zaac.201900349

[22] Narayanan, A. and Dhamodharan, R. (2015) Super Water-Absorbing New Material from Chitosan, EDTA and Urea. *Carbohydrate Polymers*, **134**, 337-343. https://doi.org/10.1016/j.carbpol.2015.08.010

[23] Janković, B., Stopić, S., Bogović, J. and Friedrich, B. (2014) Kinetic and Thermodynamic Investigations of Non-Isothermal Decomposition Process of a Commercial Silver Nitrate in an Argon Atmosphere Used as the Precursors for Ultrasonic Spray Pyrolysis (USP): The Mechanistic Approach. *Chemical Engineering and Processing: Process Intensification*, **82**, 71-87. https://doi.org/10.1016/j.cep.2014.06.002

[24] Magdalena, A.G., Silva, I.M.B., Marques, R.F.C., Pipi, A.R.F., Lisboa-Filho, P.N. and Jafelicci, M. (2018) Edta-Functionalized Fe_3O_4 Nanoparticles. *Journal of Physics and Chemistry of Solids*, **113**, 5-10. https://doi.org/10.1016/j.jpcs.2017.10.002

[25] Augustine, R., Kalarikkal, N. and Thomas, S. (2013) A Facile and Rapid Method for

the Black Pepper Leaf Mediated Green Synthesis of Silver Nanoparticles and the Antimicrobial Study. *Applied Nanoscience*, **4**, 809-818. https://doi.org/10.1007/s13204-013-0260-7

[26] Garcia, E.E., Albitres, G.A.V., Freitas, D.F.S., Mariano, D.M. and Mendes, L.C. (2023) Dyeability of Composite Based on Recycled Poly(ethylene Terephthalate) Filled with Pristine and Zinc/Silver-Modifying Titanium Phosphate. *Fibers and Polymers*, **25**, 577-586. https://doi.org/10.1007/s12221-023-00437-9

[27] Prestch, E., Buhlmann, P. and Affolter, C. (2000) Structure Determination of Organic Compounds. Springer.

[28] Estevez, M.B., Raffaelli, S., Mitchell, S.G., Faccio, R. and Alborés, S. (2020) Biofilm Eradication Using Biogenic Silver Nanoparticles. *Molecules*, **25**, Article 2023. https://doi.org/10.3390/molecules25092023

[29] Saravanan, M., Arokiyaraj, S., Lakshmi, T. and Pugazhendhi, A. (2018) Synthesis of Silver Nanoparticles from Phenerochaete Chrysosporium (MTCC-787) and Their Antibacterial Activity against Human Pathogenic Bacteria. *Microbial Pathogenesis*, **117**, 68-72. https://doi.org/10.1016/j.micpath.2018.02.008

[30] Kim, J.S., Kuk, E., Yu, K.N., Kim, J., Park, S.J., Lee, H.J., *et al*. (2007) Antimicrobial Effects of Silver Nanoparticles. *Nanomedicine*: *Nanotechnology*, *Biology and Medicine*, **3**, 95-101. https://doi.org/10.1016/j.nano.2006.12.001

[31] Rahisuddin, AL-Thabaiti, S.A., Khan, Z. and Manzoor, N. (2015) Biosynthesis of Silver Nanoparticles and Its Antibacterial and Antifungal Activities towards Gram-Positive, Gram-Negative Bacterial Strains and Different Species of Candida Fungus. *Bioprocess and Biosystems Engineering*, **38**, 1773-1781. https://doi.org/10.1007/s00449-015-1418-3

[32] Manimaran, K., Yanto, D.H.Y., Anita, S.H., Nurhayat, O.D., Selvaraj, K., Basavarajappa, S., *et al*. (2023) Synthesis and Characterization of Hypsizygus Ulmarius Extract Mediated Silver Nanoparticles (AgNPs) and Test Their Potentiality on Antimicrobial and Anticancer Effects. *Environmental Research*, **235**, Article 116671. https://doi.org/10.1016/j.envres.2023.116671

[33] Gandhi, M. and Chikindas, M.L. (2007) Listeria: A Foodborne Pathogen That Knows How to Survive. *International Journal of Food Microbiology*, **113**, 1-15. https://doi.org/10.1016/j.ijfoodmicro.2006.07.008

[34] Belluco, S., Losasso, C., Patuzzi, I., Rigo, L., Conficoni, D., Gallocchio, F., *et al*. (2016) Silver as Antibacterial toward Listeria Monocytogenes. *Frontiers in Microbiology*, **7**, Article 307. https://doi.org/10.3389/fmicb.2016.00307

[35] Mohammed, A.N. and Abdel Aziz, S.A.A. (2018) Novel Approach for Controlling Resistant Listeria Monocytogenes to Antimicrobials Using Different Disinfectants Types Loaded on Silver Nanoparticles (AgNPs). *Environmental Science and Pollution Research*, **26**, 1954-1961. https://doi.org/10.1007/s11356-018-3773-5